Astronomy & Astrophysics

Desorption rates and sticking coefficients for CO and N$_2$ interstellar ices[*]

S. E. Bisschop[1], H. J. Fraser[2], K. I. Öberg[1,3], E. F. van Dishoeck[1], and S. Schlemmer[4]

[1] Raymond and Beverly Sackler Laboratory for Astrophysics at Leiden Observatory, Postbus 9513, 2300 RA Leiden, The Netherlands
   e-mail: bisschop@strw.leidenuniv.nl
[2] Department of Physics, University of Strathclyde, 107 Rottenrow East, Glasgow G4 ONG, Scotland
[3] Division of Geological and Planetary Sciences, California Institute of Technology, Mail Stop 150-21, Pasadena, CA 91125, USA
[4] I. Physikalisches Institut, Universität zu Köln, Zulpicher Strasse 77, 50937 Köln, Germany

ABSTRACT

We present Temperature Programmed Desorption (TPD) experiments of CO and N$_2$ ices in pure, layered and mixed morphologies at various ice "thicknesses" and abundance ratios as well as simultaneously taken Reflection Absorption Infrared Spectra (RAIRS) of CO. A kinetic model has been developed to constrain the binding energies of CO and N$_2$ in both pure and mixed environments and to derive the kinetics for desorption, mixing and segregation. For mixed ices N$_2$ desorption occurs in a single step whereas for layered ices it proceeds in two steps, one corresponding to N$_2$ desorption from a pure N$_2$ ice environment and one corresponding to desorption from a mixed ice environment. The latter is dominant for astrophysically relevant ice "thicknesses". The ratio of the binding energies, R_{BE}, for pure N$_2$ and CO is found to be 0.936 ± 0.03, and to be close to 1 for mixed ice fractions. The model is applied to astrophysically relevant conditions for cold pre-stellar cores and for protostars which start to heat their surroundings. The importance of treating CO desorption with zeroth rather than first order kinetics is shown. The experiments also provide lower limits of 0.87 ± 0.05 for the sticking probabilities of CO-CO, N$_2$-CO and N$_2$-N$_2$ ices at 14 K. The combined results from the desorption experiments, the kinetic model, and the sticking probability data lead to the conclusion that these solid-state processes of CO and N$_2$ are very similar under astrophysically relevant conditions. This conclusion affects the explanations for the observed anti-correlations of gaseous CO and N$_2$H$^+$ in pre-stellar and protostellar cores.

Key words. astrochemistry – molecular processes – methods: laboratory – ISM: molecules – ISM: clouds

1. Introduction

CO and N$_2$ are two of the most abundant species in molecular clouds and therefore control the abundances of many other molecules. CO is the second most abundant molecule after H$_2$, both in the gas phase and in the solid state. Gaseous CO abundances up to 2.7×10^{-4} with respect to H$_2$ are found in warm regions (Lacy et al. 1994), indicating that CO contains most of the carbon not locked up in refractory material. In cold clouds, CO ice absorption features are seen superposed on the spectra of background sources or embedded protostars (e.g., Chiar et al. 1994; Pontoppidan et al. 2003). The solid CO abundance varies strongly from source to source, but can be as high as 10^{-4} with respect to H$_2$ in the coldest cores (Pontoppidan et al. 2005). Such high abundances are consistent with indirect determinations of the amount of CO frozen out in the densest parts of pre-stellar cores based on submillimeter line and continuum data, which suggest that more than 90% of the CO is

removed from the gas (e.g., Caselli et al. 1999; Tafalla et al. 2004; Jørgensen et al. 2005).

The amount of N$_2$ present in the gas and solid state is more uncertain, since N$_2$ cannot be detected directly as it lacks a permanent dipole moment. The abundance of gas phase N$_2$ is usually inferred from the presence of the daughter species N$_2$H$^+$. Early work by Womack et al. (1992) inferred gas phase N$_2$ abundances of $2-6 \times 10^{-6}$ with respect to H$_2$ in star-forming regions, indicating that N$_2$ contains at most 10% of the nitrogen abundance. Up to an order of magnitude higher abundances were found by van Dishoeck et al. (1992), suggesting that at least in some sources the transformation to molecular form is complete. More recent determinations of the N$_2$ abundance have focused on dark cores for which the physical structure is well determined from complementary data. For example, Bergin et al. (1995) and Bergin et al. (2002) find typical gas-phase N$_2$ abundances of $1-2 \times 10^{-5}$. Indirect indications for N$_2$ freeze-out onto grains can be obtained from analysis of the millimeter N$_2$H$^+$ data, which suggest a decline in the gas-phase abundance by a at least a factor of two in the centers of dense cores (Bergin et al. 2002;

---

[*] Appendix is only available in electronic form at http://www.edpsciences.org

Belloche & André 2004). Constraints on the amount of solid N_2 that might be present come from analysis of the solid CO band profile (Elsila et al. 1997). The most stringent limits indicate that the N_2:CO ratio must be less than 1:1, derived for sources for which both [12]CO and [13]CO ices have been detected (Boogert et al. 2002; Pontoppidan et al. 2003). This limit only holds for mixed ices of CO and N_2, not when N_2 ice has formed a separate layer.

The chemistries of CO, N_2 and their daughter products are intimately linked, even though the two molecules belong to different elemental families. This is due to the fact that CO is one of the main destroyers of N_2H^+ in the gas phase. When CO is frozen out onto the grains, N_2H^+ is enhanced, as confirmed observationally by the anti-correlation of the abundances of N_2H^+ with CO and HCO^+ in pre- and protostellar regions (Bergin et al. 2001; Tafalla et al. 2002; Di Francesco et al. 2004; Pagani et al. 2005; Jørgensen 2004). This anti-correlation is often quantitatively explained by a factor of 0.65 difference in the binding energies for CO and N_2, allowing N_2 to stay in the gas phase while CO is frozen out. These models do not contain an active grain-surface chemistry, but only include freeze-out and desorption. The relative freeze-out behavior of CO and N_2 also affects the abundance of H_3^+ and its level of deuterium fractionation (Roberts et al. 2002). Indeed, observations of H_2D^+ in cold cores and in protoplanetary disks often invoke large (relative) depletions of CO and N_2 (Ceccarelli & Dominik 2005).

The above discussion clearly indicates the need for a good understanding of the processes by which CO and N_2 freeze-out and desorb from the grains under astrophysically relevant conditions. To describe desorption, accurate values for the binding energies and the kinetics of the process are needed. For freeze-out, the sticking probability is the main uncertainty entering the equations. In an earlier paper (Öberg et al. 2005, hereafter Paper I), we presented a limited set of experiments using our new ultra-high vacuum (UHV) set-up to show that the ratio of the binding energies R_{BE} for CO and N_2 in mixed and layered ices is at least 0.923 ± 0.003 and in many circumstances close to unity. This result can be understood chemically by the fact that the two molecules are iso-electronic. Indeed, the sublimation enthalpies calculated from the IUPAC accredited data for pure ices were found to be 756 ± 5 K and 826 ± 5 K for pure N_2 and CO ices respectively, giving a ratio of 0.915 (Lide 2002). This experimental ratio is much larger than the value $R_{BE} = 0.65$ adopted in chemical models to explain the observational data (Bergin & Langer 1997; Ceccarelli & Dominik 2005). In an alternative approach, Flower et al. (2005) used the results from Paper I and instead varied the sticking probabilities of CO and N_2, which were assumed to be 1 below 15 K in all previous models. They could only reproduce the observed anti-correlation of N_2H^+ and HCO^+ if the sticking probability for N_2 was lowered to 0.1 compared with 1 for all other molecules.

In this paper, we present new experiments on CO–N_2 ices, both in pure, layered and mixed ice morphologies with varying ice "thicknesses" and relative abundances. In addition to TPD, RAIRS is used to probe the mixing, segregation and desorption processes in the ices. The aim of these experiments is to understand the CO–N_2 ice system to an extent that the

experimental desorption kinetics can be modeled and reproduced, and to subsequently use these model parameters to predict the behavior of CO and N_2 under astrophysically relevant conditions. The key parameters to be derived for the CO–N_2 ice are: i) the CO-CO, CO-N_2, and N_2-N_2 binding energies, ii) the desorption kinetics (i.e., the desorption rates), iii) the diffusion kinetics (i.e., the mixing and segregation rates), and iv) lower limits to the sticking probabilities.

This paper is organized as follows: Sect. 2 focuses on the experimental procedure and choice of ice layers and mixtures, Sect. 3 presents the experimental results on desorption, Sect. 4 a kinetic model of the experimental data, and Sect. 5 experiments on the sticking probabilities. Section 6 discusses how the kinetic model can be applied to astrophysically relevant situations and predicts the desorption behavior of CO and N_2 for astrophysically relevant heating rates. In Sect. 7 all important conclusions are summarized.

2. Experimental procedure

The experimental apparatus used for this work, CRYOPAD (Cryogenic Photoproduct Analysis Device) (van Broekhuizen 2005), is very similar to the SURFRESIDE Leiden surface astrochemistry instrument described in detail elsewhere (Fraser & van Dishoeck 2004). Briefly, all experiments were performed in an ultra-high vacuum (UHV) chamber, capable of reaching base pressures of better than 1×10^{-10} Torr. At the center of the chamber is a gold-coated copper substrate, mounted in close thermal contact with a closed cycle He cryostat, which cools the whole substrate to 14 K. The cryostat and substrate assembly is mounted on a rotation stage which can be rotated through 360 deg. The sample temperature is controlled to better than ± 0.1 K using the cryostat cold finger, a resistive heating element and a Lakeshore 340 temperature control unit. The system temperature is monitored with two KP-type (0.07% Au in Fe versus chromel) thermocouples, one mounted on the substrate face, the second by the heater element. Ices are grown in situ onto the substrate, by exposing the cold surface to a steady flow of gas, introduced into the chamber via an all metal flow control valve, with a modified outlet directed at the substrate center, along the surface normal. TPD is induced by heating the substrate (and ice sample) at a steady rate of 0.0017 K s^{-1}, using a linear heating ramp controlled by a positive feedback loop from the Lakeshore instrument. The ice film is monitored using FT-RAIRS (Fourier Transform RAIRS), which is an analysis technique providing information on the orientation and constituents of the ice film. The RAIR spectra cannot be directly compared to observational data, however, since they differ from transmission spectra. During flow setting, deposition and desorption, gases liberated from the surface are monitored using a quadrupole mass spectrometer (Pfeiffer Prisma).

To enable CO and N_2 to be discriminated from each other (and the background signal) with mass spectrometry, isotopes of both molecules were used, i.e. [13]CO (Icon Isotopes 99.998% $m/e = 29$), and [15]N_2 (Cambridge Isotopes Inc. 98% $m/e = 30$). This isotopic substitution is simply an experimental asset and does not affect the results presented in Sect. 3: [12]CO

and ^{14}N$_2$ will behave identically. In the pure and layered ice morphologies, the gases were used as supplied; to form the mixed ices a 1:1 gas mixture of ^{13}CO:^{15}N$_2$ was pre-prepared and mounted on the UHV chamber gas-dosing system. The dosing rate for ice-film growth was set prior to cooling the sample, by sequentially backfilling the chamber with the gas(es) of interest, to a pressure of around 1×10^{-8} Torr, equivalent to an ion reading on the mass spectrometer of 7.5×10^{-10} A for both ^{15}N$_2$ and ^{13}CO. The flow was then stopped, and the background pressure within the chamber allowed to recover to $\approx 1 \times 10^{-10}$ Torr, before the sample was cooled to 14 K. A background RAIRS spectrum was recorded prior to ice growth. The ice films were then grown by reopening the preset flow valve for exposure times equivalent to the gas dose required per sample gas (see Table 1), according to the morphology of the ice to be grown, assuming 1 L (Langmuir) is $\approx 1 \times 10^{-6}$ Torr s^{-1}, which roughly corresponds to ~ 1 monolayer per unit area (cm^2) of material on the substrate. In the remainder of this paper, the ices are discussed in terms of the gas exposure (in L) to which the substrate was subjected during ice-growth; for quick conversion to astronomically relevant surface concentrations, it can be assumed that a direct relationship exists between the "exposure" value quoted, and surface coverage or "thickness" of the resulting ice, which will be approximately n monolayers of material, assuming an exposure of n L and a surface concentration of 10^{15} molecules cm^{-2}.

During film growth, the CO-gas uptake on the cold surface was monitored directly with RAIRS (see Fig. 1) and indirectly by detecting residual CO and N$_2$ gas with the mass spectrometer. Since N$_2$ has no permanent dipole, it is infrared inactive and can only be monitored with the mass spectrometer. CO ice growth was initially seen to be non-linear (Fig. 1), most probably due to the preferential formation of isolated "islands" of CO on the substrate (as is for example also seen by Nekrylova et al. 1993) rather than an even, flat "thin-film" of CO-ice, where the substrate surface is fully saturated. Around 40 L, CO ice growth becomes linear, indicating that the structure of the ice that is forming no longer changes during deposition and the ice is present as a "thin-film". This is a key reason for using an ice thickness of 40 L CO for experiments in which the relative abundance of N$_2$ is varied. The ice was then heated in a TPD experiment (for a detailed discussion of TPD experiments see e.g., Menzel 1982), and 1 cm^{-1} resolution RAIR spectra were recorded as the temperature reached ≈ 15, 20, 22, 24, 25, 26, 27, 28, 29, 30, 35 and 40 K.

The ice samples studied are summarized in Table 1. Throughout this paper, the notation X/Y indicates a layered ice morphology with X on top of Y, whereas X:Y denotes a fully mixed ice system. The 1/1 and 1:1 notation denotes identical amounts of both species, whereas the x/40 L notation refers to experiments in which the "thickness" of the overlying N$_2$ layers is varied, but that of the CO layer is kept constant at 40 L. The "thicknesses" have been chosen to be of astrophysical relevance: if all condensible carbon were frozen out as CO it would form an ice layer equivalent to $\sim$40 monolayers on an interstellar grain (Pontoppidan et al. 2003). This is a fortuitous coincidence with the point at which, experimentally, thin-film CO-ice growth dominates in our apparatus. A layered

Table 1. Overview of ice morphologies and ice exposure used in the experiments.

	^{13}CO L^a	^{15}N$_2$ L^a	Total L^a
Pure ^{13}CO	20	–	20
	40	–	40^b
	80	–	80
Pure ^{15}N$_2$	–	20	20
	–	40	40^b
	–	80	80
^{13}CO-^{15}N$_2$	10	10	20
	20	20	40
	40	40	80^b
	80	80	160
^{13}CO/^{15}N$_2$	10	10	20
	40	40	80^b
	80	80	160
^{15}N$_2$/^{13}CO	10	10	20
	20	20	40
	40	40	80^b
	80	80	160
	5	40	45
	10	40	50
	20	40	60
	30	40	70
	50	40	90

^{a} In Langmuir (see Sect. 2).
^{b} Data previously reported in Paper I.

ice morphology is indicated by analysis of the interstellar solid CO profiles, which reveal a component of pure CO ice which contains 60−90% of the total solid CO abundance and which is clearly separated from the H$_2$O ice (Tielens et al. 1991; Chiar et al. 1994; Pontoppidan et al. 2003). Chemical models show that nitrogen is transformed into N$_2$ at later times and at higher extinctions when compared with the conversion of carbon from atomic form into CO (d'Hendecourt et al. 1985; Hasegawa et al. 1992). Thus, either CO starts freezing out before N$_2$ is formed so that N$_2$ forms a "pure" overlayer, or both molecules are present in the gas phase and freeze out together. This makes N$_2$/CO and N$_2$:CO the most astrophysically relevant ice morphologies to study; CO/N$_2$ ices were however also included in this study, to complete our understanding of the behavior of the ice systems. In terms of relative abundances, observational evidence (Sect. 1) suggests that the N$_2$ abundance is always less than or equal to that of CO. Models including gas-grain chemistry predict N$_2$ ice abundances that are typically a factor 5−20 lower than those of CO ice (Hasegawa & Herbst 1993; Shalabiea & Greenberg 1994; Bergin et al. 1995; Aikawa et al. 2005). Together, these arguments led to the choice of ice morphologies and exposures summarized in Table 1.
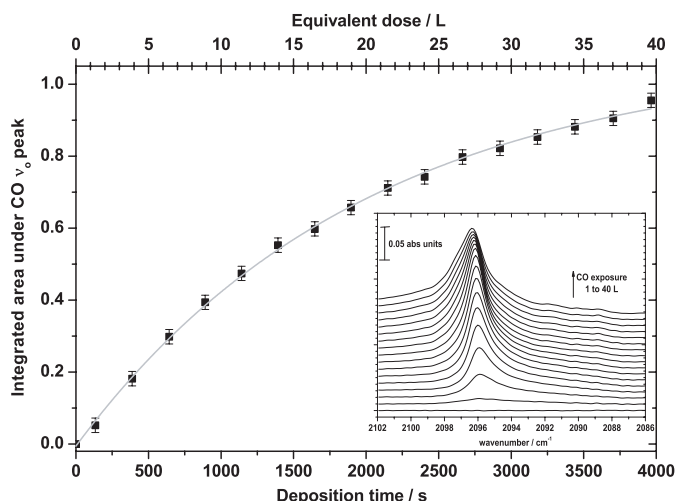
Fig. 1. Integrated intensity of the ^{13}CO RAIR spectra with deposition time. Individual RAIR spectra are shown in the inset for ice exposures of 1 to 40 L in steps of 3 L (Langmuir).

3. Experimental results

3.1. Pure CO and N₂ ices

In Figs. 2a and c, the TPD spectra for three different ice exposures, i.e. 20, 40, and 80 L, for pure CO and N₂ ices are shown. The CO TPD curves indicate that the onset for desorption is at around 26 K in the laboratory. The leading edges of the TPD curves for the 40 and 80 L exposures overlap, suggesting that the desorption process occurs at a rate that is independent of the ice thickness. Consequently the peak of the CO TPD curve shifts to higher temperatures for increasing ice thicknesses, peaking at 28 K for an exposure of 40 L. This indicates the presence of multilayer films, since the number of molecules that desorb depends only upon the number of molecules in the surface, which is identical at ice exposures of 40 and 80 L. Thus the desorption rate is constant until there are no molecules left on the surface and desorption stops. This type of kinetics is called zeroth order kinetics. The order of the kinetics is defined as the power of the number of molecules in the surface with which the rate of desorption scales (for details see Sect. 4.1). Since the differences in the CO TPD spectra are smaller for all ice morphologies, this is the only time they are discussed (Fig. 2a). The TPD signal for the 20 L experiment has a lower intensity than expected from scaling the 40 L data. This is due to island growth at low exposures (see Fig. 1 and Sect. 2).

The onset of N₂ desorption shifts from 25 K for 20 and 40 L exposures, to 24 K for 80 L (see Fig. 2c). The peak position of N₂ remains the same for the 40 and 80 L experiments. This indicates that in contrast to CO, the desorption rate of N₂ increases with increasing ice thickness. This kind of kinetics is called first order kinetics. Note that, in general, desorption kinetics do not have to have an exact integer value. For example Bolina et al. (2005) find that multilayer desorption of CH₃OH on highly oriented pyrolytic graphite (HOPG) has a desorption order of 0.35. In most cases, however, the desorption kinetics will approach either zeroth, first or even second order.

RAIRS data for pure ^{13}CO 20, 40 and 80 L exposures are shown in the first row of Fig. 3. The peak position is around 2096 cm^{-1} with a full width half maximum of 2 cm^{-1}. When the temperature increases above ∼20 K, a reduction in intensity and narrowing is observed on the blue side of the CO band. This change is probably due to restructuring of the ice. It is likely that the initial ballistic deposition results in an "open" amorphous ice structure; at around 20 K the CO molecules become torsionally mobile about their lattice points, resulting in an "on the spot" rotation about each molecule's center of mass, and the formation of a more closely packed structure. Finally, around 26 K when pure CO ice starts desorbing, more dramatic changes occur in the CO band. The origin of these changes is thought to be due to crystallization and is described in more detail in a future publication. The intensity decreases due to desorption, and a small peak grows on the blue side of the main feature.

3.2. Layered ices

The N₂ TPD spectra for the 1/1 N₂/CO experiments and x/40 L N₂/CO are shown in Figs. 4a and c respectively. Additionally, the 1/1 experiments of CO/N₂ are shown in Fig. 5. In all cases at least one peak is observed in the TPD spectra, but from the majority of the data it is evident that the TPD spectra are actually composed of two peaks, one at around 26 K (labeled peak I) and one at around 28 K (labeled peak II). In all the spectra, peak I coincides with the position of the TPD desorption peak in pure N₂, so it is attributed to N₂ desorbing from a pure N₂ layer; peak II coincides with the position of the pure CO TPD desorption peak and is therefore assigned to co-desorption of N₂ with CO, hypothesizing this occurs from a mixed phase of CO-N₂ ice. The formation of this mixture would require bulk diffusion of N₂ and/or CO between the two separate layers. This mobility is found to commence at significantly higher temperatures than those expected for the hopping process on surfaces (Tielens & Allamandola 1987). The energy-barrier to hopping is typically assumed to be 0.3× the binding energy, corresponding to around ∼285 K for CO and N₂ and implying that CO and N₂ are mobile around 10 K. Our much higher temperature for mobility is probably due to a much larger barrier to bulk diffusion than for surface diffusion. For comparison, experiments by Collings et al. (2003) suggest CO molecules become mobile at around 12−15 K on both CO and H₂O-ice surfaces, suggesting the barrier to surface diffusion is only slightly higher than the theoretical approximation used in astrochemical models. Furthermore it is clear that the mixing process occurs during ice annealing, and not immediately on deposition, first because there is significant N₂ desorption from a pure ice phase and second because the desorption profiles of the layered and mixed ice systems differ significantly (see Sect. 3.3).

Important information about the CO-N₂ ice system can be derived from the relative intensities of peak I and II. In the 1/1 and x/40 L N₂/CO experiments, a turnover is observed between the peak intensities (see Figs. 4a and c), with peak II being more intense than peak I for low "thickness", and
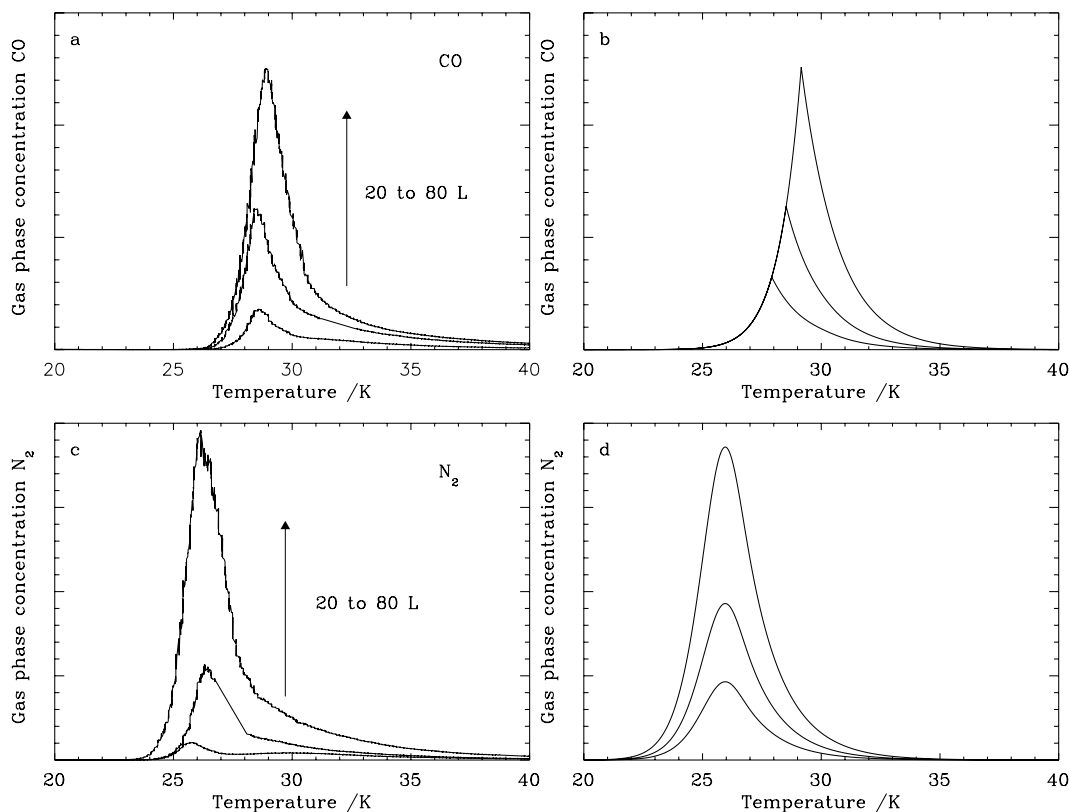
Fig. 2. TPD spectra for pure ices with exposures of 20, 40, 80 L. **a)** CO experiments, **b)** CO model, **c)** N₂ experiments, and **d)** N₂ model.

visa versa at high "thickness". This turn-over occurs between the 40/40 L and 60/60 L exposures for the 1/1 experiments, and between the 30/40 L and 50/40 L in the x/40 L experiments, i.e. both sets of experiments consistently have the turn-over point around 40/40 L.

The CO RAIR spectra of the layered ices (second and third rows of Fig. 3) have a ^{13}CO feature that is almost identical to that for pure ^{13}CO, although the red-wing is less pronounced. As for pure CO, the intensity of the blue-wing decreases around 20 K, where the ice restructures, and a new peak grows around 26 K, where CO starts to desorb. Since the changes in the layered ice spectra at 20 K are commensurate with similar changes in the pure CO ice spectra, this is unlikely to be an indicator of the mixing process. Additionally, a blue wing appears around 24−25 K, concurrently to the onset of N₂ desorption in the TPD spectra (see Fig. 4). This feature is probably due to mixing of both molecules, as will be discussed in Sect. 4.3. The appearance of a blue wing around 24 K rather than 20 K reaffirms that the mixing process relies on bulk rather than surface diffusion.

Finally, the TPD spectra of 1/1 CO/N₂ ice layers at exposures of 20, 80 and 160 L are shown in Fig. 5. These experiments were used primarily to test whether the ices were indeed grown as separate layers on top of each other. The turn-over point where peak I becomes more intense than peak II occurs at slightly higher exposures compared with N₂/CO ice layers, i.e. between 40/40 L and 80/80 L. It is therefore clear that N₂ desorption is retarded by the CO overlayer, desorbing only after it has mixed with, and (a fraction of which has) subsequently

segregated from, the CO-ice. As the spectra do not resemble those of the pure N₂ ice, these experiments provide positive evidence that the layer growth is sequential and coincident on the substrate. However, this ice structure is not thought to be astrophysically relevant, so it is not discussed further in this article.

3.3. Mixed ices

The N₂ TPD spectra for mixed ices (Fig 4e) differ from those of pure or layered ices in that only one peak is observed, skewed to the low, and not high temperature side of the desorption range. As the "thickness" of the mixed ice increases, the TPD peak maximum shifts from 28 to 26 K. This behavior indicates that at low exposures, N₂ desorbs predominantly from a mixed-ice environment, whereas as the exposure increases, a more significant fraction of the N₂ is able to desorb form a pure N₂ layer. Furthermore, the TPD peaks are broadened with respect to those observed for pure and layered ice morphologies (see Sects. 3.1 and 3.2). This broadening is likely to be due to the merging of peaks I and II, and the potential for a wider range of binding environments to exist in the intimately mixed ice morphology. Desorption occurring from a pure N₂ ice environment suggests that segregation must also occur within mixed CO-N₂ ice systems, including the mixed phases that are formed in the layered ice systems. However the fact that some desorption from the mixed phase is always observed indicates that the segregation happens at a lower rate than the mixing process, potentially because the energy barrier to segregation is greater than that for mixing. This would
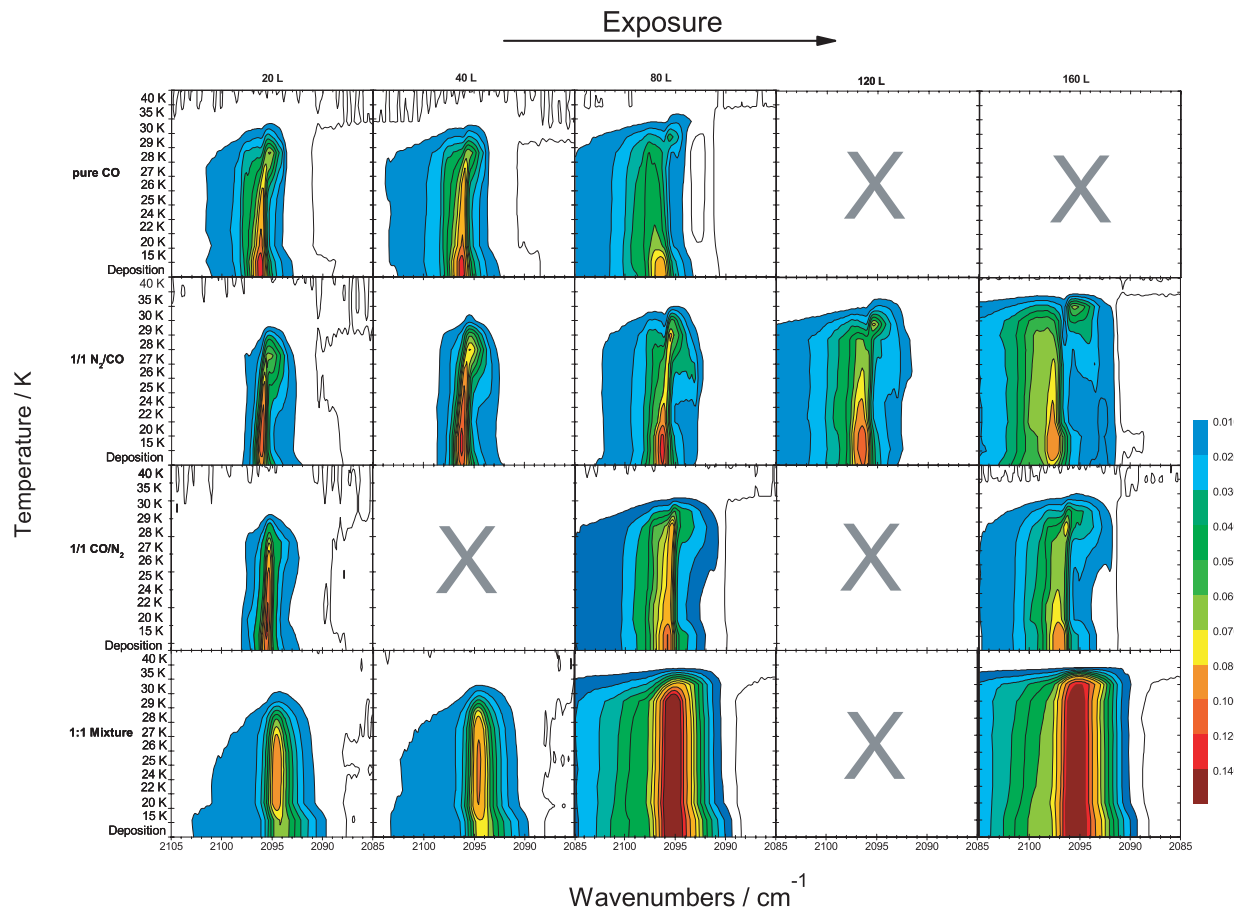
Exposure

Fig. 3. 2-D RAIR spectra of ^{13}CO plotted as frequency vs. temperature (on a non-linear temperature scale), in pure CO, mixed and layered CO:N$_2$ ices, with exposures indicated at the top of the matrix and ice morphologies on the left hand side. X = data not available.

suggest that over certain temperature ranges the mixed ice phase is thermodynamically more stable than the segregated layers.

The RAIR spectra of the mixed ices (final row Fig. 3) differ from those of the pure and layered ices, being broader (4 cm^{-1}) and shifted to 2094 cm^{-1}, reflecting, as with the TPD data, that the structure of the mixed ices is unique. Again, the CO band changes shape at around 20 K, possibly due to a similar restructuring as observed for the pure and layered ices, discussed in Sects. 3.1 and 3.2, but no further changes are observed as the temperature increases until the ice starts desorbing. This implies that all or most of the CO remains in a mixed ice phase until it starts to desorb; even if the concentration of this phase changes slightly as the N$_2$ segregates and desorbs, it is not evident in the RAIR spectra.

4. Empirical model of CO-N$_2$ desorption

A model was built to gain a clearer qualitative and quantitative understanding of the thermal annealing processes including diffusion, mixing and desorption of the ices. The aims of this model are twofold; to reproduce the experimental data and then apply the same kinetic parameters to astrophysically relevant ice morphologies, temperatures and heating rates.

4.1. Constructing the model

The kinetic processes for desorption, mixing and segregation in this system have a reaction barrier (i.e. they are thermodynamically limited) and can therefore be described by the following equation:

$$r_{\mathrm{des}} = \frac{\mathrm{d}N}{\mathrm{d}t} = \nu_i [N_{\mathrm{s}}]^i \mathrm{e}^{-E/T} \tag{1}$$

where r_{des} is the desorption rate (molecules cm^{-2} s^{-1}), N is the number of molecules evaporating from the substrate (assuming throughout the remainder of these calculations that the substrate has unit surface area (cm^2)), t is time in s, ν_i the pre-exponential factor (molecules^{1-i} cm$^{2(i-1)}$ s^{-1}), i is the reaction order, $[N_{\mathrm{s}}]$ is the number of molecules partaking in a particular reaction per unit surface area (molecules cm^{-2}), E is the reaction barrier in K, which for the desorption processes can be read as the binding energy, and T is temperature in K. The physical meaning of the pre-exponential factor ν_i depends upon the reaction order i. For a first order reaction it refers to the lattice vibrational frequency which is typically in the range 10^{11}–10^{13} s^{-1}; for zeroth order desorption it consists of the product of the lattice vibrational frequency with the surface density of order 10^{15} molecules cm^{-2}. Depending on the type of reaction, the reaction order i can vary, taking positive, negative and any non-integer real value. Both E and ν_i depend
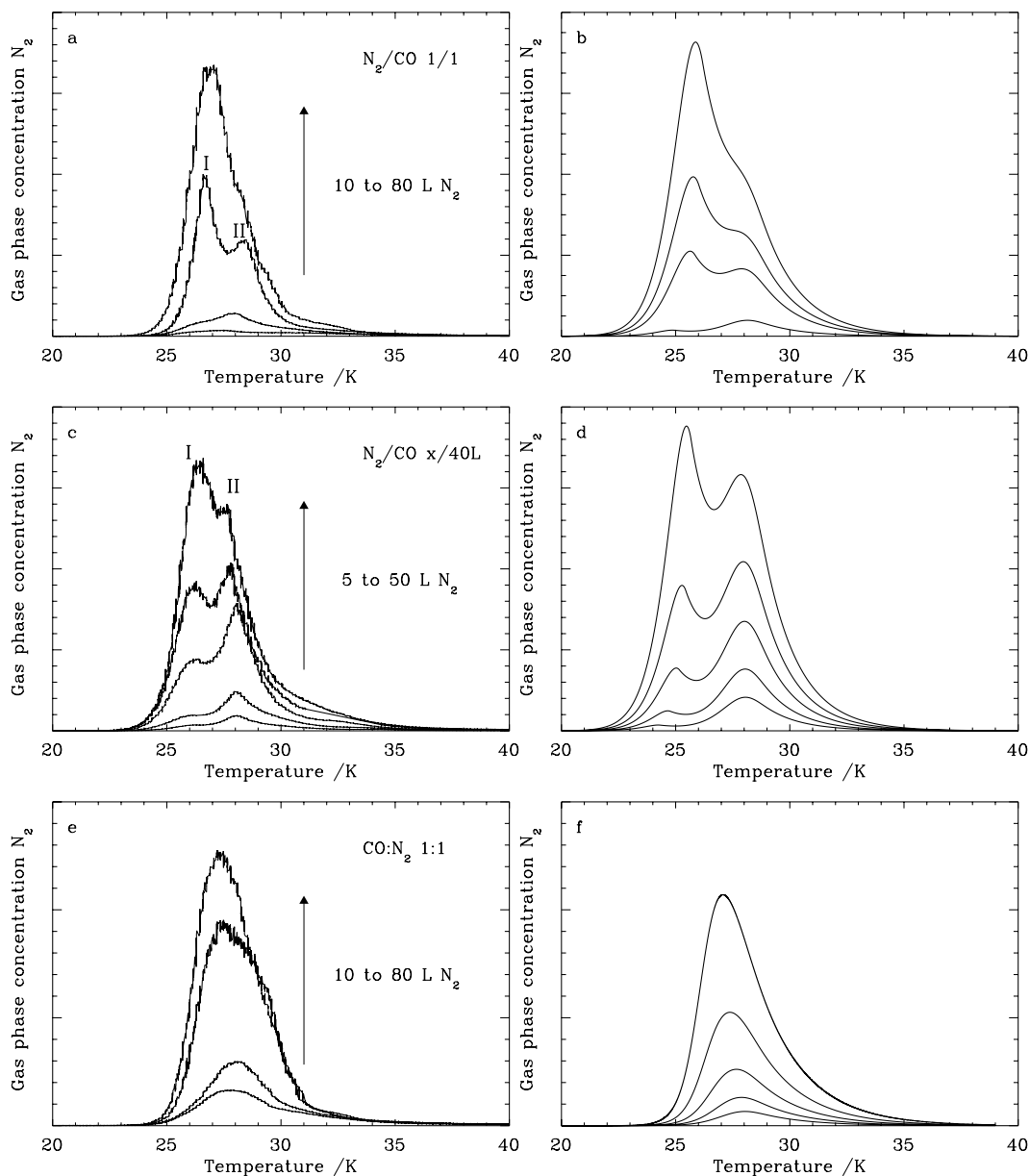
Fig. 4. N$_2$ TPD spectra: **a)** (10-20-40-80 L)N$_2$/(10-20-40-80 L)CO, 1/1 layer, **c)** (5-10-20-30-50 L)N$_2$/(40 L)CO, differential layer, **e)** (10-20-40-80 L)N$_2$:(10-20-40-80 L)CO, mixed ice 1:1. The equivalent model spectra are shown in **b)**, **d)**, and **f)**, respectively. The two experimental TPD peaks are labeled I and II, corresponding to desorption of N$_2$ from pure and mixed ice phases respectively.

in principle upon "thickness". However, this dependence is not thought to be large since no major changes are observed between the FTIR spectra at different coverages indicating that the intermolecular environments are very similar.

In order to calculate the temperature-dependent rate measured in the TPD experiments, the following conversion needs to be made:

$$\frac{dN}{dt} = \frac{dN}{dT}\frac{dT}{dt} \tag{2}$$

where dN/dT is the temperature-dependent rate (molecules cm^{-2} K^{-1}), and dT/dt the TPD heating rate (K s^{-1}). At each time step, a fraction of the molecules that have evaporated into the gas phase will be removed by the pump;

subtracting this rate from the desorption into the gas phase will reproduce the experimental conditions. The pump-rate is given by:

$$r_{\text{pump}} = \frac{dN}{dt} = -\nu_{\text{pump}}N(g) \tag{3}$$

in which ν_{pump} is the pump constant in s^{-1} and $N(g)$ the number of molecules entering the gas phase having desorbed from a unit surface area. To ensure the equations balance, $N(g)$ is given in molecules cm^{-2}, implying that the molecules actually occupy a unit volume. Combining Eqs. (1)−(3), the experimental results can be simulated in a simple way. The reactions are summarized in Table 2.

Table 2. Rate equations for desorption, mixing, and segregation of CO and N_2 in the CO-N_2 ice systems.

	Reaction	Rate equation	ν (molecules$^{(1-i)}$ cm$^{2(i-1)}$ s^{-1})	E (K)	i
a	$CO(s) \rightarrow CO(g)$	$\nu_0 e^{-E/T}$	$7.0 \times 10^{26 \pm 1, a}$	855 ± 25	0
b	$N_2(s) \rightarrow N_2(g)$	$\nu_1 [N(s)]^i e^{-E/T}$	$1.0 \times 10^{11 \pm 1}$	800 ± 25	1
c	$CO(mix) \rightarrow CO(g)$	$\nu_1 [CO(mix)]^i e^{-E/T}$	$7.0 \times 10^{11 \pm 1}$	930 ± 25	1
d	$N_2(mix) \rightarrow N_2(g)$	$\nu_1 [N_2(mix)]^i e^{-E/T}$	$1.0 \times 10^{12 \pm 1}$	930 ± 25	1
e	$CO(s) \rightarrow CO(mix)$	$\nu_0 e^{-E/T}$	$5.0 \times 10^{26 \pm 1}$	775 ± 25	0
f	$N_2(s) \rightarrow N_2(mix)$	$\nu_0 e^{-E/T}$	$5.0 \times 10^{26 \pm 1}$	775 ± 25	0
g	$CO(mix) + N_2(mix) \rightarrow CO(s) + N_2(s)$	$\nu_2 [CO(mix)][N_2(mix)] e^{-E/T}$	$1.0 \times 10^{-4 \pm 1}$	930 ± 25	2
h	$CO(g) \rightarrow CO(pump)$	$\nu_{pump} [CO(g)]$	$1.0 \times 10^{-3, a}$	–	1
i	$N_2(g) \rightarrow N_2(pump)$	$\nu_{pump} [N_2(pump)]$	$8.2 \times 10^{-4, a}$	–	1

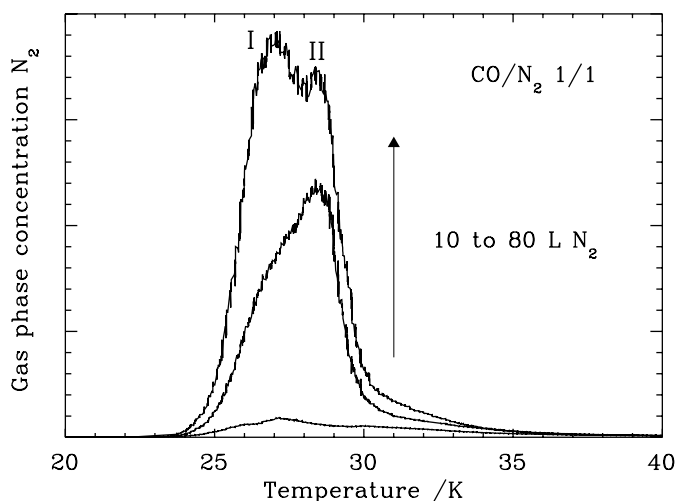[a] Parameters are fixed according to experimental constraints see Sect. 4.2.

Fig. 5. N_2 TPD spectra of (10-40-80 L)CO/(10-40-80 L)N_2, 1/1 layer. The two experimental TPD peaks are labeled I and II, corresponding to desorption of N_2 from pure and mixed ice phases respectively.

4.2. Constraining the model

First, the reactions h and i given in Table 2 plus the pump constants ν_{pump} for CO and N_2 were constrained, by fitting a first-order exponential to the pump-down curves of both CO and N_2 at 14 K, accounting for the pumping effects of the turbo-pump and the cryostat in the experiment. Note that the ν_{pump} values shown in Table 2 are experimentally determined and consequently fixed for further iterations of the kinetic model.

Next, the parameters associated with reactions a and b, desorption from pure ice environments, were constrained. Since the binding energies for pure CO ice desorption found by Collings et al. (2003) and Paper I are identical within experimental error, the CO binding energy was initially set to the same value reported in Paper I; ν was fixed at the value reported by Collings et al. (2003). For N_2, the desorption kinetics appear to be first order (see Sect. 3.1) and therefore the pre-exponential factor ν was initially estimated to be somewhere between 10^{11}–10^{13} s^{-1}, then varied in order to obtain the best fit to the experimental data. The N_2 binding energy was initially

set to the value reported in Paper I, but also allowed to vary in iterations of the model. The final values of these parameters are given in Table 2 and the corresponding TPD models are presented next to the experimental data in Figs. 2b and d.

Desorption from the mixed ice fraction was assumed to be first order. This is thought to be a good assumption since the rate of desorption depends on the number of molecules on the surface and this will change after each molecule desorbs. Initially, the binding energy for desorption from the mixed ice layer was taken to be the same as that of pure CO desorption, because peak II appears to occur at the same temperature as the desorption of pure CO. However, when running the model this value had to be increased to reproduce the experimental effect.

From the TPD spectra described in Sect. 3 no direct measurement of the mixing rates was possible. Mixing can, however, be inferred from the presence of peak II in the layered ice experiments. Assuming a simple, single step process, reactions e and f in Table 2 describe the mixing, assuming both molecules contribute equally to the process. Good physical arguments can be made for modeling this process as zeroth, first or second order kinetics, and all three processes were investigated (see Appendix A for a more detailed discussion). The outcome is that experimental data are best reproduced if the mixing process is zeroth order. Since mixing occurs only at the interface between the CO and N_2 ice layers this description makes physical sense. A CO or N_2 molecule at the interface has a certain chance of overcoming the "mixing barrier" and diffusing into the opposite layer, but the molecules remaining at the interface will still see the same number of molecules, regardless of whether there are 20 or 80 L of ice above or below it.

The final reaction to constrain is the segregation reaction g. The relative number of molecules desorbing from pure N_2 environments in mixed ice morphologies increases with exposure, as was discussed in Sect. 3.3. Segregation is modeled as one reaction, in a second order process depending on the initial number of molecules in the mixed ice phase for both species. In reproducing all the mixed ice experiments these values were, of course, equal. In the layered ices, however, it is unlikely that the relative abundances of CO and N_2 in the mixed ice phases are equal. Consequently, equation g suggests that

segregation is fastest from an equimolar ice, decreasing as the relative abundances of either species deviate from 1:1. Finally, from the TPD spectra of the layered ices it was clear that the mixing was more efficient than the segregation process, so, as discussed in Sect. 3.2, the E of reaction g was always assumed to be greater than E of reactions e and f.

4.3. Results

In Table 2, all the model equations and best fit parameters "by eye" are given after running a large number of models. The error-bars arise from (i) the range of values over which simultaneous fits of ν and E gave degenerate solutions to the model, (ii) the uncertainty in the number of molecules present on the surface, and (iii) the experimental uncertainties in the temperature. It is important to realize that the degeneracy in the simultaneous fits of ν and E means that the combination of these values is more accurate than the individual values. Thus, in astrochemical models both parameters need to be used in combination to accurately reproduce the behavior of CO and N$_2$.

A comparison between Figs. 2a and c with Figs. 2b and d clearly shows that the model described here very reasonably reproduces the data of the pure CO and N$_2$ ice system. The leading edges for the CO TPD spectra of the experiment do not quite overlap as perfectly as the model does, probably because CO desorption is close to, but not quite, zeroth order. As was discussed by Collings et al. (2003) the error resulting from this deviation from zeroth order is significantly smaller than all other errors made in astrochemical models. The best-fitted parameters for E are 855 K and 800 K for CO and N$_2$ respectively.

The desorption peaks I and II observed in the TPD spectra for the layered ices are also well reproduced by the model. The appearance of peak II depends on equations c and d which describe desorption of CO and N$_2$ from the mixed ice phase. From Table 2 it is seen that ν and E are within the model error-bars identical in each reaction, confirming that N$_2$ and CO co-desorb from this mixed ice phase. Since E from the mixed ice is greater than E from the pure ice, it seems CO and N$_2$ are both more strongly bound in the mixed ice. The results give a R_{BE} of 0.936 ± 0.03 for the pure N$_2$ and CO ices and 1.0 for the mixed ices, within experimental error of Paper I. Note that even for layered ices of "thicknesses" less than 40 L, most N$_2$ desorbs from a mixed ice environment.

Mixing kinetics were confirmed to be zeroth order. The best-fit E value equals 775 K, which is rather close to E found for desorption of pure N$_2$ and indicates that significant mixing only occurs close to desorption of N$_2$, corresponding to the change in RAIR spectra found around 24 K in Sect. 3.2. This behavior is also illustrated in Fig. 6a for the 20/40 L N$_2$/CO experiment, where the growth of the mixed ice phase is commensurate with the loss of the pure ice phase and the desorption of the pure N$_2$ layer. For higher ice thicknesses of N$_2$, the competition between mixing and desorption is in favor of desorption from the pure ice layer, leading to the turn-over in peak intensity from peak I and II.

Segregation starts close to the desorption temperature of CO, which is illustrated by Fig. 6b for the 20:20 L CO:N$_2$
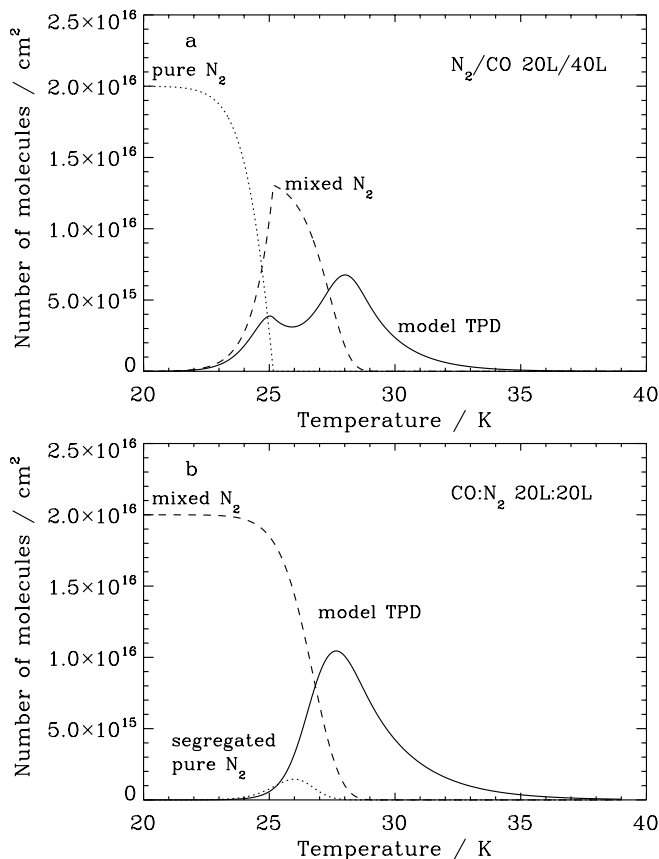

Fig. 6. Model results for the ice and gas phase concentrations as functions of temperature. The number of molecules in pure N$_2$ ice (dotted line), in mixed ice (dashed line), and in the gas phase (solid line) are shown for 20/40 L N$_2$/CO **a)** and the 20:20 L CO:N$_2$ **b)**.

experiment. This occurs at a higher temperature than the onset of mixing, due to a barrier difference; E equals 930 K for segregation and 775 K for mixing. This difference makes segregation a relatively unimportant process for layered ices. As for mixed ices, however, the segregation rate increases with ice thickness, leading to a larger segregated fraction for higher initial ice thickness, which shifts the TPD peak to lower temperatures.

5. Sticking probability

The data presented so far are key to our understanding of CO and N$_2$ desorption rates in interstellar environments. However, because the binding energies of CO and N$_2$ in the solid phase are essentially so similar, this parameter cannot be the main factor which accounts for the anti-correlation of N$_2$H$^+$ with CO and HCO$^+$ in pre-stellar cores. The freeze-out rate, or a difference in the sticking probability of each molecule to the grain, may also be relevant.

Without a molecular beam facility, it is very difficult to quantify sticking probabilities directly. Nevertheless, during these experiments, the gas load reaching the mass spectrometer was monitored during the flow setting for a time period equivalent to the dosing period (when the substrate was warm) and the entire dosing period (when the substrate was cold).

Table 3. Lower limits to the sticking probabilities at 14 K.

System	Sticking probability
CO → CO	≥0.9 ± 0.05
N$_2$ → N$_2$	≥0.85 ± 0.05
N$_2$ → CO	≥0.87 ± 0.05

By combining the measurements over a range of deposition times and experiments, it is possible to extract a value for the uptake coefficient. From the uptake coefficient only a lower limit to the sticking probability can be derived since the mass spectrometer signal at low temperatures also includes an unknown fraction of molecules that miss the substrate (for a more detailed explanation of the derivation of the uptake coefficient see Fuchs et al. 2006). The uptake coefficient at surface temperatures of 14 K is given by

$$S(\theta) = \frac{\int N_x^w \mathrm{d}t - \int N_x^c \mathrm{d}t}{\int N_x^w \mathrm{d}t} \qquad (4)$$

where θ is the "thickness" in L, and $\int N$ is the integrated area under the mass spectrometer signal for species x during the dosing period, warm (w) or cold (c), respectively, which is directly proportional to the fraction of molecules that do not stick, i.e. either they never reach the substrate, scatter from the surface without sticking, or are trapped and desorb on a very short timescale (<1 s).

However, since the sticking probability is dependent of ice "thickness" and ice morphology, the growth of islands or non-linear thin films during deposition, such as is observed in these experiments (see Fig. 1), results in the sticking probability changing as a function of ice "thickness", tending exponentially (in this case) towards a constant (lower value) at flat, multilayer ice thicknesses (Kolanski 2001). To determine this "constant" S-value for CO sticking to CO, N$_2$ sticking to N$_2$, and N$_2$ sticking to CO, the S-values were plotted as a function of exposure (in L), and fitted to an exponential decay curve, for every experiment where the final ice morphology was identical. The asymptotic values of S are given in Table 3. The errors on the uptake coefficients, i.e., the lower limits of the sticking probabilities, arise from a combination of the reproducibility of the experiments plus the error bar on the fitted exponential decay curve.

It is clear that at 14 K these values are identical within experimental error, averaging 0.87 ± 0.05. The values given in Table 3 represent the lower limits to the sticking probabilities at surface temperatures of 14 K; at higher ice thicknesses these values will not change, and at lower ice thicknesses they tend exponentially towards 1. In our experiments, the non-unity sticking probability may arise because the gases are dosed effusively into the chamber at 300 K, even though the substrate itself is at 14 K.

Based on comparison with other systems it is expected that for a single molecule incident upon any of these surfaces, the sticking probability will tend towards 1, particularly as its incident energy is reduced from 300 to 100 or even 10 K, and

the surface temperature of the ice is reduced to 10 K. The data clearly show that the relative differences between the S-values of CO-CO, N$_2$-N$_2$ and N$_2$-CO are negligible relative to other uncertainties in astrochemical models, and are certainly not as large as one order of magnitude, as adopted by Flower et al. (2005).

6. Astrophysical implications

The model described in Sect. 4 can be refined to simulate the behavior of CO-N$_2$ ices in astrophysical environments, simply by replacing the heating rate used in the experiment with an appropriate heating rate for the astrophysical conditions and removing the pumping reactions.

Figure 7a shows output of the astrophysical model for 1/1 layered N$_2$/CO ices (solid lines), at heating rates of 1 K/1000 yr. This heating rate was chosen because it matches the timescale over which a newly-formed protostar increases the temperature in its surrounding envelope from <10 K to 20 K (Lee et al. 2004). In addition, the desorption profiles of pure N$_2$ and CO in layered ice are shown on the same plot. Under these conditions, pure N$_2$ desorbs between 15 and 17 K, ∼2 K or 2000 yr earlier than CO, which desorbs between 17 and 19 K. However, if N$_2$ were to freeze-out on top of an existing CO-ice layer, the desorption of N$_2$ takes place in two steps. Only for unrealistically thick ices of more than 80−120 monolayers does 50% of N$_2$ desorb as pure N$_2$. For lower ice thicknesses, N$_2$ desorption from the mixed environment dominates, and the majority of the frozen-out N$_2$ desorbs with CO. Figure 7b shows a very similar plot, but for 1:1 mixed ices, where the desorption occurs in a single step. As the total ice thickness increases, i.e. more CO and N$_2$ are equally frozen out, the desorption profile shifts towards the pure N$_2$ case, but generally the profile resembles that of pure CO much more closely than that of pure N$_2$. It is important to note that the thermodynamics, i.e. R_{BE} of the CO and N$_2$ ice systems have not been altered in any of these models; the differences arise entirely from the kinetics of the desorption processes. This illustrates that it is important to know the initial morphology of the ice as well the abundance of N$_2$ with respect to CO to make accurate predictions for the interstellar desorption behavior of N$_2$ compared to CO.

Many astrochemical models use first order desorption kinetics for pure CO instead of zeroth order kinetics (e.g., Ceccarelli & Dominik 2005). To get an impression of the magnitude of the error made by using incorrect desorption kinetics, a simulation for pure CO desorption from an ice of 40 L was made for both cases using identical binding energies (see Fig. 7c). Clearly, desorption for first order kinetics occurs ∼1 K or 1000 yr earlier, corresponding to an error of 12.5% on the desorption timescale. Although this seems a small overall error, it is 50% of the time difference between desorption of pure N$_2$ and CO, so this incorrect treatment could have a comparatively large effect on the relative desorption behavior of layered ices of N$_2$ and CO. It is also important to notice that CO desorption in pure CO ice is completed ∼0.5 K earlier than desorption of CO from a mixed or layered ice environment. This is due to
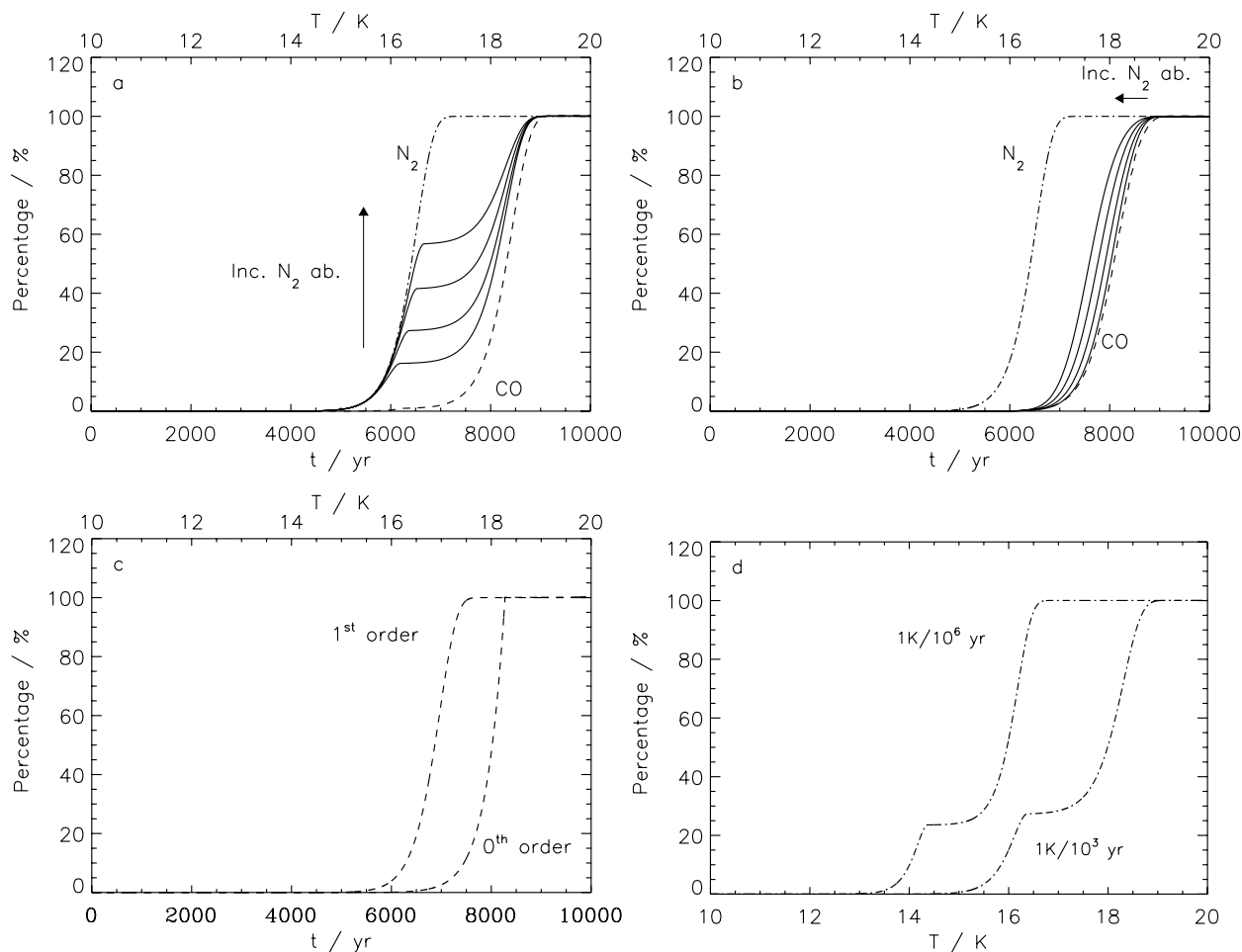
Fig. 7. Astrophysical simulations for heating rates of 1 K/ 10^3 yr with ice thicknesses ranging from 10 to 80 L for both species. **a)** (10-20-40-80 L)N$_2$/(10-20-40-80 L)CO, 1/1 layer, **b)** (10-20-40-80 L)N$_2$:(10-20-40-80 L)CO, 1:1 mixed ice; **c)** zeroth and first-order desorption for 40 L pure CO, and **d)** a simulation for N$_2$/CO 20/40 L for heating rates of 1 K/ 10^3 yr and 1 K/ 10^6 yr. N$_2$ desorption from the mixed or layered ices is shown in full, pure N$_2$ in dash-dot, and CO in dashed lines.

the lower surface concentration of CO in a mixed ice environment as was found in the experiments.

In Fig. 7d, the difference between heating rates of 1 K/ 10^3 yr and 1 K/10^6 yr is shown for an ice with 20/40 L N$_2$/CO. The relevance of the faster rate was defined previously; the slower rate would be appropriate for a cold pre-stellar core at near constant temperature. It is clear that the qualitative picture remains the same; N$_2$ desorbs in two steps, but desorption is complete by 16.5 K for 1 K/10^6 yr versus at 18.5 K for 1 K/1000 yr, a difference of 2 K for a difference in heating rate of 10^3. One further issue is that at the lower heating rates a slightly greater fraction of the N$_2$ desorbs from a mixed ice environment, which implies that the mixing rate becomes faster relative to the desorption rate. An infinitely slow heating rate of 1 K/ 10^{10} yr shows the same trend.

The overall conclusion from our experiments is that there are some subtle differences in the N$_2$ and CO desorption behavior, but that they are unlikely to fully explain the observed anti-correlations between N$_2$H$^+$ and CO in pre-stellar dense cores. Also, any difference in sticking probabilities for CO and N$_2$ is

very small, so that other scenarios must be explored to explain the observations.

So far, H$_2$O ice has been neglected in our studies. The CO-H$_2$O system has been extensively studied by Collings et al. (2003), who found a binding energy of CO to H$_2$O of 1180 K. Kimmel et al. (2001) derive a binding energy of ≥950 K for N$_2$ on H$_2$O. The combination of these two results in a R_{BE} on H$_2$O of ≥0.81. Furthermore, Manca et al. (2004) and Manca & Martin (2003) report a ratio for the condensation enthalpies on H$_2$O of 0.83. Concluding, R_{BE} on H$_2$O for CO and N$_2$ is very close to that found for the binary CO-N$_2$ system. The desorption behavior will thus also be quite similar for CO and N$_2$ in mixed or layered ices with H$_2$O as is observed in the TPD experiments by Collings et al. (2004), where both species desorb in multiple steps. The addition of H$_2$O to the CO-N$_2$ ice system therefore could not significantly alter the conclusions of this paper. A significant difference in binding energies between CO and N$_2$ could only occur if most of the CO were residing in a H$_2$O-dominated environment with N$_2$ in a pure, separate layer on top. This would be in contradiction with the

observations which show that a large fraction of the CO is in a pure CO ice layer (Pontoppidan et al. 2003).

Modifications to the gas-phase chemistry are an alternative possibility to explain the observations. For example, Rawlings et al. (2002) show that a higher initial H/H$_2$ ratio can affect the relative N$_2$H$^+$ and HCO$^+$ abundances in cores where the chemistry has not yet reached equilibrium. Even in models including freeze-out, there are regimes of densities and temperatures where the N$_2$H$^+$ abundance initially rises as CO and N$_2$ freeze out. Dissociative recombination with electrons then becomes the dominant N$_2$H$^+$ destruction mechanism (Jørgensen et al. 2004), leading mostly to NH rather than N$_2$ (Geppert et al. 2004). Eventually, this results in N$_2$H$^+$ depletion at high densities and later times.

7. Concluding remarks

New experimental data have been presented for the desorption and sticking of CO-N$_2$ ice systems. Furthermore a kinetic model has been constructed that allows for accurate simulations of the TPD experiments as well as predictions for the behavior of CO and N$_2$ ices under astrophysical conditions. The key results are:

- The ratio for the binding energies for N$_2$ and CO in pure ices is 0.936±0.03. For mixed ices, the ratio for the binding energies is 1.0 (see Sect. 4.3).
- Desorption of N$_2$ from layered ices occurs in two steps, due to mixing of N$_2$ with CO. This indicates that for astrophysically relevant ice abundances, desorption from the mixed layer dominates, with less than 50% of N$_2$ able to desorb prior to CO.
- In mixed ices, segregation causes the peak temperature for N$_2$ desorption to shift to lower temperatures for higher ice thicknesses, even though most of the ice desorbs from a mixed ice environment. Since the onset of segregation is concurrent with desorption, a single broad desorption step is observed for N$_2$. For astrophysically relevant ice thicknesses, N$_2$ desorption occurs close to the CO desorption temperature.
- The desorption kinetics for CO ice are zeroth order instead of the commonly adopted first order process, resulting in an error in the desorption timescale of 12.5%, with a shift to lower temperatures for the first order process. Since this corresponds to 50% of the difference between N$_2$ and CO desorption, it results in a comparatively large effect on the relative desorption behavior of layered ices of N$_2$ and CO.
- The lower limits on the sticking probabilities for N$_2$ and CO are found to be the same within experimental error, 0.87±0.05 at 14 K (see Sect. 5). In reality the sticking probabilities will be even closer to 1.0 for lower temperatures.

The main conclusion from this work is that the solid-state processes of CO and N$_2$ are very similar under astrophysically relevant conditions.

References

Aikawa, Y., Herbst, E., Roberts, H., & Caselli, P. 2005, ApJ, 620, 330
Belloche, A., & André, P. 2004, A&A, 419, L35
Bergin, E. A., & Langer, W. D. 1997, ApJ, 486, 316
Bergin, E. A., Langer, W. D., & Goldsmith, P. F. 1995, ApJ, 441, 222
Bergin, E. A., Ciardi, D. R., Lada, C. J., Alves, J., & Lada, E. A. 2001, ApJ, 557, 209
Bergin, E. A., Alves, J., Huard, T., & Lada, C. J. 2002, ApJ, 570, L101
Bolina, A. S., Wolff, A. J., & Brown, W. A. 2005, J. Chem. Phys., 122, 4713
Boogert, A. C. A., Blake, G. A., & Tielens, A. G. G. M. 2002, ApJ, 577, 271
Caselli, P., Walmsley, C. M., Tafalla, M., Dore, L., & Myers, P. C. 1999, ApJ, 523, L165
Ceccarelli, C., & Dominik, C. 2005, A&A, 440, 583
Chiar, J. E., Adamson, A. J., Kerr, T. H., & Whittet, D. C. B. 1994, ApJ, 426, 240
Collings, M. P., Dever, J. W., Fraser, H. J., & McCoustra, M. R. S. 2003, Ap&SS, 285, 633
Collings, M. P., Anderson, M. A., Chen, R., et al. 2004, MNRAS, 354, 1133
d'Hendecourt, L. B., Allamandola, L. J., & Greenberg, J. M. 1985, A&A, 152, 130
Di Francesco, J., André, P., & Myers, P. C. 2004, ApJ, 617, 425
Elsila, J., Allamandola, L. J., & Sandford, S. A. 1997, ApJ, 479, 818
Flower, D. R., Pineau Des Forêts, G., & Walmsley, C. M. 2005, A&A, 436, 933
Fraser, H. J., & van Dishoeck, E. F. 2004, Adv. Space Res., 33, 14
Fuchs, G. W., Acharyya, K., Bisschop, S. E., et al. 2006, submitted to Faraday Discussions
Geppert, W. D., Thomas, R., Semaniak, J., et al. 2004, ApJ, 609, 459
Hasegawa, T. I., & Herbst, E. 1993, MNRAS, 263, 589
Hasegawa, T. I., Herbst, E., & Leung, C. M. 1992, ApJS, 82, 167
Jørgensen, J. K. 2004, A&A, 424, 589
Jørgensen, J. K., Hogerheijde, M. R., van Dishoeck, E. F., Blake, G. A., & Schöier, F. L. 2004, A&A, 413, 993
Jørgensen, J. K., Schöier, F. L., & van Dishoeck, E. F. 2005, A&A, 435, 177
Kimmel, G. A., Stevenson, K. P., Dohnálek, Z., Smith, R. S., & Kay, B. D. 2001, J. Chem. Phys., 114, 5284
Kolanski, K. W. 2001, Surface Science (Wiley), 163
Lacy, J. H., Knacke, R., Geballe, T. R., & Tokunaga, A. T. 1994, ApJ, 428, L69
Lee, J.-E., Bergin, E. A., & Evans, N. J. 2005, ApJ, 617, 360
Lide, D. R. 2002, CRC Handbook of chemistry and physics: a ready-reference book of chemical and physical data, 83rd edn. (CRC Press)
Manca, C., Martin, C., & Roubin, P. 2004, Chem. Phys., 300, 53
Manca, C., Martin, C., & Roubin, P. 2003, J. Phys. Chem. B, 107, 8929
Menzel, D. 1982, Chemistry and Physics of Solid Surfaces IV, ed. R. Vanselow, & R. Howe (Springer-Verlag), 389

Nekrylova, J. V., French, C., Artsyukhovick, A. N., Ukraintsev, V. A., & Harrison, I. 1993, Surface Science Letters, 295, L987

Öberg, K. I., van Broekhuizen, F., Fraser, H. J., et al. 2005, ApJ, 621, L33

Pagani, L., Pardo, J.-R., Apponi, A. J., Bacmann, A., & Cabrit, S. 2005, A&A, 429, 181

Pontoppidan, K. M., Fraser, H. J., Dartois, E., et al. 2003, A&A, 408, 981

Pontoppidan, K. M., Dullemond, C. P., van Dishoeck, E. F., et al. 2005, ApJ, 622, 463

Rawlings, J. M. C., Hartquist, T. W., Williams, D. A., & Falle, S. A. E. G. 2002, A&A, 391, 681

Roberts, H., Fuller, G. A., Millar, T. J., Hatchell, J., & Buckle, J. V. 2002, A&A, 381, 1026

Shalabiea, O. M., & Greenberg, J. M. 1994, A&A, 290, 266

Tafalla, M., Myers, P. C., Caselli, P., Walmsley, C. M., & Comito, C. 2002, ApJ, 569, 815

Tafalla, M., Myers, P. C., Caselli, P., & Walmsley, C. M. 2004, A&A, 416, 191

Tielens, A. G. G. M., & Allamandola, L. J. 1987, in ASSL 134: Interstellar Processes, ed. D. J. Hollenbach, & J. Thronson, 397

Tielens, A. G. G. M., Tokunaga, A. T., Geballe, T. R., & Baas, F. 1991, ApJ, 381, 181

van Broekhuizen, F. 2005, Ph.D. Thesis, Leiden University

van Dishoeck, E. F., Phillips, T. G., Keene, J., & Blake, G. A. 1992, A&A, 261, L13

Womack, M., Ziurys, L. M., & Wyckoff, S. 1992, ApJ, 393, 188

Online Material

Appendix A: Comparison between zeroth, first and second order mixing

Since there is no direct measurement of the mixing rate in our experiment, the correct description of mixing kinetics is derived from comparison of models for zeroth, first and second order mixing kinetics with the TPD data. All three mechanisms are physically relevant. Zeroth order can be viewed as a process in which a molecule at the interface between CO and N$_2$ has a certain chance of moving into the overlying layer; the chance for this to occur is completely independent of whether there are 20 or 80 L on top of this molecule and thus the mixing process is "thickness" independent. First order mixing would be possible in case mixing of one species with another is independent of the total number of molecules of the other species, i.e. there is no saturation possible. Second-order reactions are possible if the rate of mixing would depend upon both the total number of CO and N$_2$ molecules, since the presence of both molecules is required for mixing. Models for all scenarios were tested in order to determine which most accurately describes the experiments.

The three different scenarios are shown for 1/1 N$_2$/CO experiments in Fig. A.1 with the best fitting parameters in Table A.1. Zeroth order mixing gives rise to a turn-over in the spectrum for the peak intensities with peak II initially being more intense than peak I. This behavior is also observed for the experimental data (see Fig. 4a). The turn-over is due to most N$_2$ molecules mixing unhindered. When the pure ice layer is depleted due to desorption and mixing, mixing stops and the remainder of the molecules desorb from the mixed ice environment. Thus mixing occurs up to higher temperatures with increasing initial ice "thickness". Desorption and mixing are therefore competing processes. This behavior is not correctly reproduced by the models for first and second-order mixing (see Figs. A.1c and e). As the initial number of molecules in the layers increases, the number of molecules in the mixed fraction of the ice also increases for first order mixing kinetics (see reaction B in Table A.1). However, this increase is proportional to the number of molecules in the pure layer, resulting in a constant ratio between peak I and II. Second order mixing behaves differently from both zeroth and first-order mixing in that the turn-over is now reversed. This is due to the rate of mixing being proportional to the number of molecules for both species. Thus at low ice "thicknesses" the rate is low and both molecules remain mostly pure, whereas for high ice "thicknesses" the rate of mixing is very high and all molecules end up in a mixed environment. A comparison between Figs. A.1a, b, and c with Fig. 4 shows clearly that the scenario for zeroth order mixing reproduces the experimental data best.

The zeroth order mixing mechanism is exemplified by comparison between the CO TPD data output from the model with the experimental data for N$_2$/CO 1/1 (Fig. A.2). Second order mixing (Fig. A.1f) produces a CO desorption spectrum that looks zeroth order. For first order mixing, a two-peak structure is observed for lower "thickness" ices and desorption is dominated by first order kinetics for higher ice "thicknesses", which is not observed in the experimental data. Zeroth order mixing kinetics are, however, able to predict the increasing overlap for the leading edges plus the slight broadening of the TPD profile with respect to the pure CO TPD spectra in Fig. 2a with increasing ice thickness observed in the experimental data fairly well.
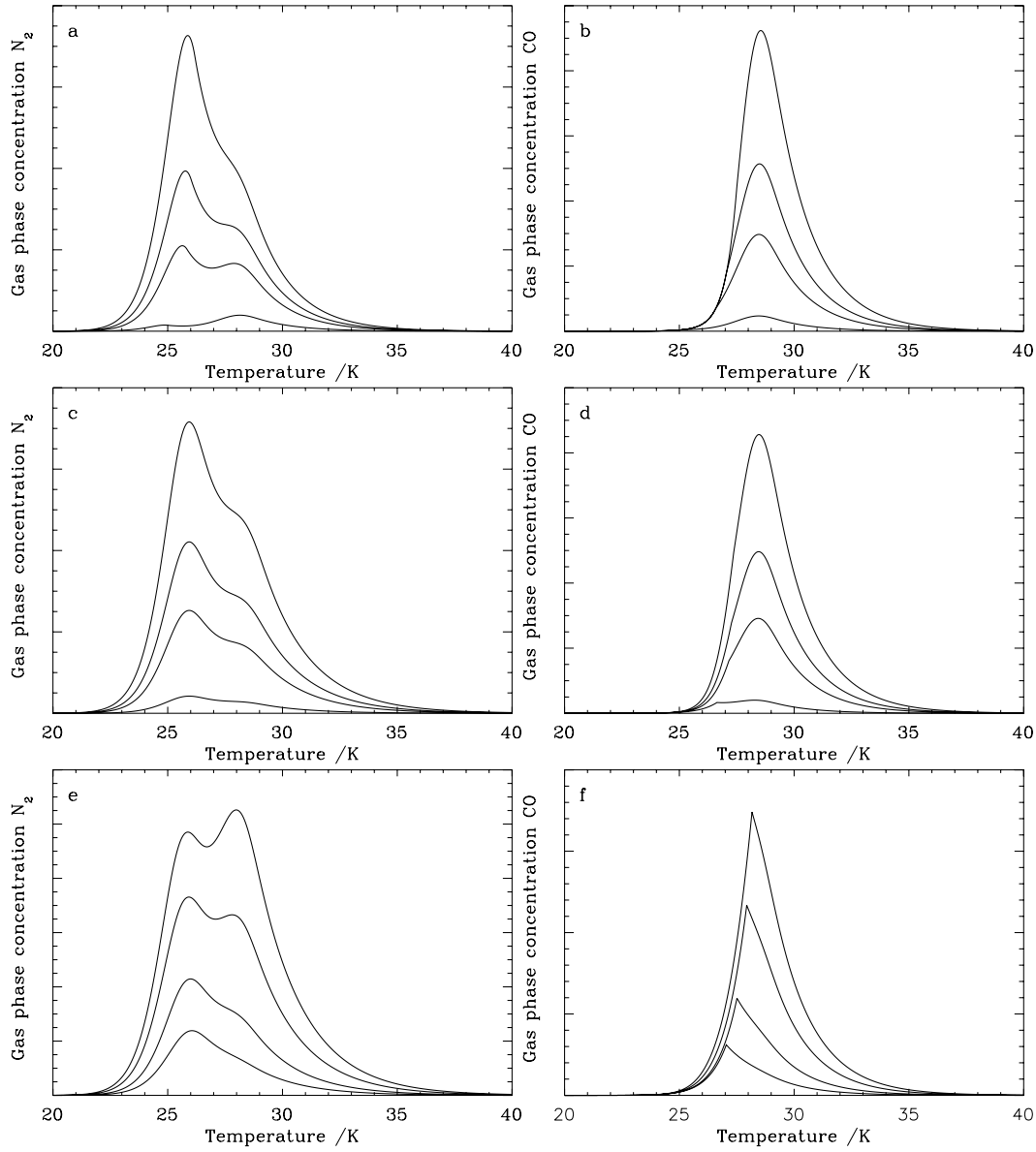
Fig. A.1. Comparison between model output for the 1/1 ices using alternative rates for mixing where **a)**+**b)** have zeroth order mixing kinetics, **c)**+**d)** first order, and **e)**+**f)** second order. N$_2$ TPD simulations are shown in **a)**, **c)**, and **e)**; CO TPD simulations are shown in **b)**, **d)**, and **f)**. The N$_2$ model results should be compared with experimental data in Fig. 4a, the CO model results with data in Fig. A.2.

Table A.1. Rate equations for the zeroth, first and second order mixing processes.

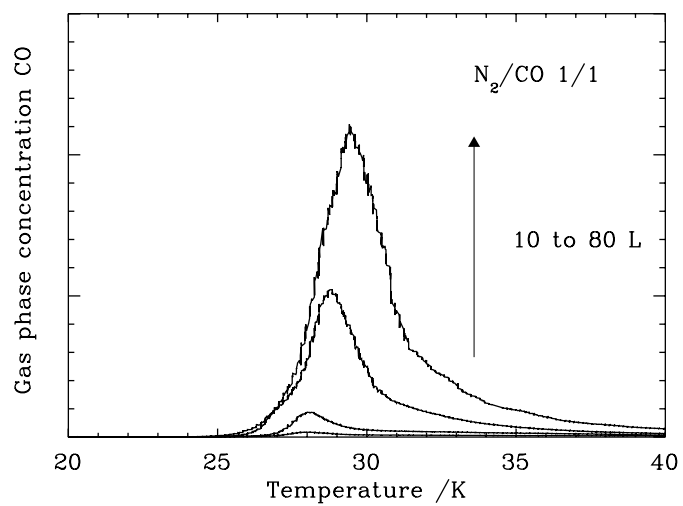|	Reaction	Rate equation	ν (molecules$^{(1-i)}$ cm$^{2(i-1)}$ s^{-1})	E (K)	i
A	CO(s)+N$_2$(s)$\rightarrow$ CO(mix)+N$_2$(mix)	$\nu_0 e^{-E/T}$	$5.0 \times 10^{26\pm1}$	775 ± 25	0
B	CO(s)+N$_2$(s)$\rightarrow$ CO(mix)+N$_2$(mix)	$\nu_1[CO(s)/N_2(s)]e^{-E/T}$	$1.0 \times 10^{12\pm1}$	885 ± 25	1
C	CO(s)+N$_2$(s)$\rightarrow$ CO(mix)+N$_2$(mix)	$\nu_2[CO(s)][N_2(s)]e^{-E/T}$	$5.0 \times 10^{-5\pm1}$	865 ± 25	2

Fig. A.2. CO TPD spectra for 1/1 (10-20-40-80 L)N$_2$/(10-20-40-80 L)CO.